BMC Cardiovascular Disorders

RESEARCH

Open Access

Impdh1 was identified as a key protein promotes diabetic vasculopathy by intervention of vascular endothelial cell pyroptosis

Ruiqiang Xie[1,2*†], Hong Gao[1,2†], Hongyan Xie[1,2], Chunguang Xie[1,2] and Tianhao Li[1*]

Abstract

Background Diabetic angiopathy (DA) is a diabetic vascular complication. Pyroptosis is an inflammatory death that plays an important role in the development of DA, but the underlying mechanisms have not been fully elucidated.

Methods The GSE169332 dataset from the Gene Expression Omnibus (GEO) was subjected to single-cell RNA sequencing (scRNA-seq) analysis, and the data of diabetic mice were subjected to bulk RNA-seq. The pathway through which the inflammatory microenvironment participated in the DA was explored by pseudotime analysis and cell-cell communication. DA models were constructed using in vitro mouse models. The histopathological changes in the collected aorta were observed by hematoxylin and eosin (H&E) and Masson staining. The distribution and expression of the phenotypic markers related to pyroptosis in aortic tissues (NLRP3, pro-Caspase1, and GSDMD-N) were observed by immunohistochemistry (IHC) or immunofluorescence (IF) staining. Following the silencing of the expression of high glucose (HG)-induced Impdh1 in endothelial cells (ECs), Impdh1 expression was detected by real-time quantitative reverse transcription PCR (qRT-PCR), and the expression of Impdh1, NLRP3, pro-Caspase1, and GSDMD was detected by IF staining; cell migration was detected by cell scratch assay, cell viability was detected by cell counting kit-8 (CCK-8) assay, and tube formation was detected by tube formation assay; the levels of IL-1β and IL-18 were detected using the enzyme-linked immunosorbent assay (ELISA) kits.

Results Impdh1 was identified by scRNA-seq and bulk RNA-seq as a key molecule in the progression of DA associated with pyroptosis of aortic ECs. By constructing mouse models of DA, it was found that silencing Impdh1 can inhibit mouse aortic pyroptosis. Silencing of the expression of HG-induced Impdh1 revealed an effective amelioration of EC damage and pyroptosis.

Conclusion Impdh1 is identified as a potential pyroptosis-related gene associated with DA by scRNA-seq of GEO data and bulk RNA-seq. Impdh1 protects aortic ECs by inhibiting pyroptosis and inflammation.

†Ruiqiang Xie and Hong Gao contributed equally to this work.

*Correspondence:
Ruiqiang Xie
xieruiqiang@cdutcm.edu.cn
Tianhao Li
litianhao_doctor@163.com

Full list of author information is available at the end of the article

Clinical trial number Not applicable.

Keywords Diabetic angiopathy, Aortic endothelial cells, Pyroptosis, Single-cell RNA sequencing, Impdh1

Background

Diabetic angiopathy (DA), one of the most serious complications of diabetes mellitus (DM), can be divided into micro- and macro-vascular angiopathy and has the clinical features of cardiovascular disease, retinopathy, nephropathy, and neuropathy, which are the main causes of morbidity and premature mortality in DM [1–3]. Some scientific studies have determined that DM is closely associated with endothelial mitochondrial dysfunction, as evidenced by increased oxidative stress, decreased biogenesis, aggravated DNA damage, and attenuated mitochondrial autophagy [4].

Inflammatory factors play a crucial role in the pathogenesis of several complications of DM. For instance, chronic inflammation is widely detected in different stages of retinopathy [5]. Inflammatory pathways play a central role in the progression of diabetic nephropathy, and the identification of new inflammatory molecules might be relevant to the development of new therapeutic strategies [6]. New research has suggested that some potential molecules targeting pyroptosis and inflammasome signaling will become new therapeutic avenues for the control and treatment of DM and its complications in the near future, demonstrating that pyroptosis exerts a crucial role in the development of DM and its complications [7].

Pyroptosis is a lytic and inflammatory type of programmed cell death usually triggered by inflammasome and executed by gasdermin (GSDM). After recognizing exogenous or endogenous signals, cells undergo inflammasome assembly, GSDM cleavage, and the release of inflammatory factors and other cellular contents, eventually resulting in inflammatory cell death. Pyroptosis is a double-edged sword that can be beneficial or harmful in various inflammatory disorders and disease conditions. The physiological outcome of these responses could be tissue damage and sometimes even death of the host, but as an immunogenic cell death, inducing pyroptotic cell death and activating strong anti-tumor immunity can be used as a new strategy for cancer elimination [8–10]. Hyperglycemia-induced endothelial damage is the most critical initial step in the development of diabetic vasculopathy during the progression of DM [11]. Mounting literature has reported that when endothelial cells are damaged, they will release and secrete numerous pro-inflammatory and pro-coagulant cytokines, inducing platelet aggregation, thrombosis, monocyte macrophage adhesion and infiltration, and the release of inflammatory factors [12]. However, long-term chronic vessel wall inflammation not only triggers endothelial cell pyroptosis but also leads to vascular dysfunction, such as impairing angiogenesis, promoting plaque formation in the arterial wall, and contributing to smooth muscle cell proliferation. These are all important pathological features of diabetic vasculopathy [13]. Thus, endothelial cell pyroptosis does play a vital role in the progression of diabetic vasculopathy.

Inosine monophosphate dehydrogenase (IMPDH) catalyzes the rate-limiting step in de novo guanine nucleotide synthesis and plays a crucial role in the growth and progression of certain tumors. Inhibition of this enzyme is associated with immune-suppressive, antiviral, and antitumor activities [14, 15]. However, there are few reports on whether IMPDH is associated with the development of diabetic vasculopathy, and the exact mechanism remains to be investigated in subsequent studies.

In the present study, the potential pyroptosis-related gene associated with DA was identified by single-cell RNA sequencing (scRNA-seq) and bulk-seq. Following the identification of the hub gene Impdh1, the effect of Impdh1 expression on endothelial cells (ECs) was verified by diabetic mouse models and cells.

Methods

scRNA-seq data

scRNA-seq data were obtained from Gene Expression Omnibus (GEO) (https://www.ncbi.nlm.nih.gov/geo/) with the accession number GSE169332, including one sample that was fed a diabetogenic diet with cholesterol (DDC) and one sample that was fed a chow diet (Chow). Some low-quality as well as low-expression genes were screened out based on the following thresholds: (1) the number of genes per cell ranged from 200 to 3,000; (2) the number of unique molecular identifiers (UMIs) ranged from 200 to 10,000; and (3) the percentage of mitochondrial gene expression was less than 10% in each cell. After filtration, there were 1,774 cells and 14,688 genes. The scRNA-seq dataset was standardized using the DDCizeData function, and 2,000 highly variable genes (HVGs) were identified using the vst method in the FindVariableFeatures function. The data were normalized using the ScaleData function and then subjected to principal component analysis (PCA) via the RuDDCA function. Principal components (PCs) were selected by visual plotting with the ElbowPlot function. Subsequently, the data were visualized using the RunUMAP function (n.neighbors = 30, dims = 1:30).

Since the data were obtained from different samples, batch corrections were conducted using the R package Harmony to avoid batch effects interfering with

downstream analyses. A shared nearest neighbor (SNN) plot was constructed using the top 30 PCs and the FindNeighbors function, and then the cells were clustered using the FindClusters function (resolution = 2). Finally, cell clusters in OA were annotated based on the previous studies, and differentially expressed genes (DEGs) between each cell type were identified using the FindAllMarkers function in Seurat (min.pct = 0.1, logfc.threshold = 0.25, retaining genes with p-values < 0.05).

Pseudotime analysis

Pseudotime trajectory analysis was carried out using Monocle (version 2.26.0. Using Monocle, all the information was imported from the Seurat object into the Monocle CDS object and then down-scaled using its DDRTree method. The resulting trajectories were plotted using the default settings.

Cell-cell communication

Intercellular communication relationships were inferred based on the R package CellChat. The underlying operational logic was as follows. First, a database of signaling molecule interactions was established manually after taking full account of the known structural composition of ligand-receptor interactions, such as multimeric ligand-receptor complexes, soluble agonists and antagonists, and stimulatory and inhibitory membrane-bound co-receptors. Next, cell state-specific signaling communication within a given scRNA-seq data was inferred using mass action models, as well as differential expression analysis and statistical tests on groups of cells. In addition, CellChat also provided multiple visualization outputs, and it can quantitatively characterize and compare intercellular communication through social network analysis tools, pattern recognition methods, and multiple learning approaches.

Communication probabilities at the signaling pathway level were calculated via CellChat by summarizing the communication probabilities for all ligand-receptor interactions associated with each signaling pathway. Due to the complex cellular communication networks, the signals sent by each subset were presented. Moreover, edge weights between different networks were compared by controlling the parameter edge.weight.max.

Animals

Eight-week-old male BKS db/db mice (N = 6, Model group) and db/m mice (N = 6, Control group) were purchased from GemPharmatech (Nanjing, China). After the mice were conditionally stabilized, the caudal vein of 24 mice was injected with lentivirus-packaged sh-Impdh1 or control-negative virus (Model + NC group and Model + sh-Impdh1 group). Lentivirus was purchased from GenePharma (Shanghai, China). Five days after the assay, the mice were euthanized by excess CO_2 inhalation. The aorta was excised, frozen by liquid nitrogen, and stored in a -80℃ refrigerator for subsequent assays. All animal assays in this study were conducted under the principles of reducing the number of animals and minimizing suffering and under the guidance of the protocols approved by the Animal Care and Use Committee of our institution. All experiments involving animals were approved by the Animals Ethics Committee of OBiO Technology (Shanghai) Corp., Ltd. (Ethics approval number: IACAC-141).

Hematoxylin and Eosin (H&E) staining

Tissue samples were embedded in paraffin and cut into 5 μm thick sections. Histopathological changes were observed by H&E staining via the kits (C0105M, Beyotime, China). Images were captured using a microscope (Olympus Corporation, Tokyo, Japan).

Masson staining

The collagen fibers of tissue samples were stained using the staining kit (C0189S, Beyotime, China) according to the standard protocols and then stained with Weigert's iron hematoxylin for 5 min. After a few seconds of differentiation with 1% acidic ethanol differentiation solution, the sections were rinsed with tap water for 30 min. Subsequently, the sections turned blue. The sections were stained with ponceau-fuchin solution for 10 min and treated with aqueous phosphomolybdic solution for 5 min. Next, the sections were counter-stained with aniline blue solution for 5 min and then treated with 1% glacial acetic acid for 1 min.

Immunofluorescence (IF) staining

The frozen aortic sections were subjected to IF staining. Fixed with 4% paraformaldehyde for 15 min, the frozen sections were permeabilized with 0.3% (v/v) Triton X-100 (P0096, Beyotime, China) in PBS for 15 min and blocked with 5% (w/v) bovine serum albumin (PC0001, Solarbio, China) for 1 h. Subsequently, the sections were incubated with the primary antibodies (Caspase-1, 1:200, ab179515, Abcam, USA; GSDMD, 1:200, ab219800, Abcam, USA; NLRP3, ab283819, 1:200, Abcam, USA) overnight at 4℃ and the secondary antibody anti-rabbit IgG (Alexa Fluor 488: Molecular Probes, Eugene, OR) on the following day at room temperature for 1 h. Following continuous overnight incubation, the nuclei were stained with DAPI. Finally, the slides were sealed with a sealing solution containing anti-Fade Mounting Medium, and the images were collected under a microscope.

Real-time quantitative reverse transcription PCR (qRT-PCR)

Total RNA was extracted from cells using the TRIzol reagent (15596026CN, Invitrogen, USA). cDNA was

synthesized from 1 mg of total RNA using the SuperScript III Reverse Transcriptase kit (18080085, Invitrogen, USA) according to the standard protocols. qRT-PCR was performed on a QuantStudio 12 K Flex RT-PCR system (Applied Biosystems, CA, USA) using the SYBR Green Master Mix kit (KAPA Biosystems) according to the manufacturer's protocols. GAPDH was used as an internal reference.

The sequences of the qRT-PCR primers were shown in Table 1.

Cell culture and grouping

Human umbilical vein endothelial cells (HUVECs) (CBP60340, ATCC, USA) were cultured in vitro and randomly assigned to the NG group (normal glucose, 5 mmol/L), HG group (25 mmol/L), NC group (100 μm NC siRNA + 25 mmol/L glucose), and Impdh1 siRNA group (100 μm Impdh1 siRNA + 25 mmol/glucose). The si-NC and Impdh1 siRNA sequences were provided by Shanghai GenePharma Co., Ltd. The cells were inoculated into 6-well plates for 24 h before transfection. When cell confluence reached about 50%, the transfection reagent and plasmids or vector complexes (200 μl) were prepared according to the protocols of the Lipofectamine 3000 Transfection Kit (11668-027, Invitrogen, USA) and mixed for transfection. After 6 h of transfection, the culture medium was changed. After 48 h of incubation, cells were collected for subsequent assays.

Cell scratch assay

HUVECs were inoculated into 6-well plates (1×10^6 cells/well). 24 h later, the HUVECs were grown to complete fusion and scraped with a 10 μl pipette tip. Subsequently, the HUVECs were cultured in a serum-free medium for 24 h. Images were obtained under a light microscope at 0 and 24 h. Cell scratch was assessed by measuring the wound distance using the Image-Pro Plus 6.0 software.

Cell counting kit-8 (CCK-8) assay

The cell viability of each group at 0, 24, 48, and 72 was detected using the CCK-8 kit (C0038, Beyotime, China), and the specific experimental steps were referred to the kit protocols.

Tube formation assay

HUVECs were cultured in high glucose (HG)-DMEM (D6429, Sigma, USA) containing 10% fetal bovine serum (FBS) and passaged at 80% cell confluence. Cells within 7 generations were best for tube formation assays. To enhance tube formation, cells can be starved the day before the assay. Each well of the pre-cooled 96-well plates was added with 50 ul of melted matrix gel and then placed in a 37℃ cell incubator for 30 min to 1 h. Cells were resuspended according to a system of approximately 2.0×10^4-3.0×10^4 cells/well and 100 ul of medium in the 96-well plates. The cell suspension was inoculated onto the solidified matrix gel. Three replicate wells were set up for each experimental group. Cells were observed 4 h after they were spread well, and images of tube formation in a bright field were directly captured using an image acquisition device.

Enzyme-linked immunosorbent assay (ELISA)

The levels of IL-1β and IL-18 in mice and HUVECs were determined using human IL-18 ELISA kit (ab215539, Abcam, USA), mouse IL-18 ELISA kit (ab216165, Abcam, USA), human IL-1 beta ELISA kit (ab214025, Abcam, USA), and mouse IL-1 beta ELISA kit (ab100705, Abcam, USA). 100 μL of standard working solution or serum samples were added to the corresponding plate wells and then incubated at 37℃ for 90 min. After the liquid was discarded, 100 μL of the working solution was immediately added and incubated at 37℃ for 60 min. Next, 100 μL of horseradish peroxidase (HRP)-coupled working solution was added to each well and incubated at 37℃ for 30 min. Finally, 90 μL of substrate solution was added and incubated at 37℃ for about 15 min. Subsequently, the reaction was stopped and the 450 nm wavelength was immediately read to process the data.

Bulk RNA-seq

Total RNA was first extracted from mouse samples. The integrity of the extracted RNA was examined by agarose gel electrophoresis, and the concentration of the RNA was precisely determined by NanoDrop. mRNA was isolated from the total RNA using magnetic beads with oligo-dT, and the captured mRNA was fragmented. The first and second strands of cDNA were then synthesized using reverse transcriptase. After the RT product was end-repaired, an A base was added to the 3' end. Subsequently, the fragment was ligated to the sequencing junction, and the ligation product was purified to remove the products with incomplete ligations and the self-linkage products with empty junctions. Next, primers

Table 1 Primers of qRT-PCR

Gene	forward	reverse
GAPDH (mouse)	5'-TGACCTCAACTACATGGTCTACA – 3'	5'- CTTCCCATTCTCGGCCTTG – 3'
Impdh1 (mouse)	5'-GGCTACGTTCCCGAGGATG-3'	5'-GCTGATGTCAGGTCCACTTCA-3'
GAPDH (human)	5'- ACAACTTTGGTATCGTGGAAGG – 3'	5'- GCCATCACGCCACAGTTTC – 3'
Impdh1 (human)	5'-CAGCAGGTGTGACGTTGAAAG-3'	5'-AGCTCATCGCAATCATTGACG-3'

complementary to the junction sequence were used for PCR amplification. Finally, the sequencing library was obtained by purification with magnetic beads. After the library was constructed, the concentration of the library was detected by Qubit, and the fragment length of the library was detected by Agilent Fragment Analyzer to ensure the quality of the library.

The raw sequencing data (Raw data) obtained at the end of sequencing were subjected to bioinformatic analysis, including sequencing data quality assessment and reference sequence alignment as well as the functional analyses of the DEGs. Sequencing data quality assessment can quickly determine if there are quality issues with the data to screen high-quality data for further analysis. Reference sequence alignment is to align the sequences after quality control to a reference genome and then to calculate gene expression abundance by annotating information with the reference genome. Differential expression analysis of genes was performed using DESeq2 to screen for DEGs. Subsequently, the DEGs were subjected to functional analyses, including Gene Ontology (GO) and Kyoto Encyclopedia of Genes and Genomes (KEGG), or analysis of variable shear events according to the experimental design scheme.

Statistical analysis

Results were expressed as mean ± standard deviation (SD). All data were analyzed using SPSS and GraphPad Prism 8.0.2. Variables between two groups were compared by the student's t-test, and variables among multiple groups were compared by the one-way ANOVA, the preferred test for conducting post hoc tests on a one-way ANOVA. $P < 0.05$ was considered significant and had statistical significance.

Results

Single-cell public dataset analysis

The clusters obtained from clustering were annotated according to the corresponding cell type markers; The UMAP plots of each cell type in the samples were shown in Fig. 1A-C. It was shown that the cells were categorized into ECs, Macrophages, Fibroblasts (Fibs), and Smooth muscle cells (SMCs). The proportions of each cell type in the two groups were shown in Fig. 1D. In the DDC group, the proportion of Macrophages was decreased, and the proportion of ECs was increased, whereas there was no significant difference in the proportions of Fibs and SMCs.

ECs were extracted for re-clustering and grouping. Using some specific markers, the ECs were classified into 2 cellular subsets, ECs_Impdh1$^+$ and ECs_Impdh1$^-$ (Fig. 1E).

Changes in gene expression during EC differentiation

For further understanding of the mechanism of EC differentiation, the potential developmental relationships and genetic changes during EC differentiation were explored by performing pseudotime analysis on the EC subsets with Monocle 2. As shown in Fig. 2A, ECs_Impdh1$^+$ was almost mostly concentrated on the end branch, with some distribution at the start branch, but the number decreased somewhat with trajectory. Whereas, ECs_Impdh1$^-$ was focused on the start branch. The trajectory plot between the DDC and Chow groups (Fig. 2B) showed that the Chow group presented the ECs_Impdh1$^-$→ECs_Impdh1$^+$ differentiation pathway.

As shown in Fig. 2C, the genetic changes during the EC differentiation were explored.

The results of cell-cell communication analysis were shown in Fig. 2D, where the signals sent by ECs_Impdh1$^+$ and ECs_Impdh1$^-$ to other cells were displayed. Gas6-Axl was specifically expressed between Impdh$^+$ subsets.

Silencing Impdh1 can inhibit aortic tissue damage and pyroptosis in mice

To test the efficiency of silencing Impdh1 in mice, Impdh1 expression was detected by qRT-PCR. It was shown in Fig. 3A that compared with the Control group, Impdh1 expression was significantly elevated in the Model and Model + NC groups, while significantly down-regulated in mice injected with sh-Impdh1. The differences were all statistically significant ($P < 0.05$). IF staining results (Fig. 3B) showed that the optical density (OD) values of NLRP3, pro-Caspase1, and GSDMD were significantly increased in the Model and Model + NC groups compared with the Control group, whereas the OD values in the Model + sh-Impdh1 group were significantly decreased compared with the Model and Model + NC groups. The results of the pathological sections are shown in Fig. 3C-D. H&E and Masson staining showed that compared with the Control group, the arterial wall of the Model group was significantly thickened; the space between the arterial media and externa was significantly narrowed; the number of infiltrating cells were significantly increased; collagen fibers were significantly thickened; and the cells were chaotically aligned and unevenly distributed. Whereas, silencing of Impdh1 markedly ameliorated the pathology of the aorta in mice, reduced infiltrating cells, and restored collagen fibers. The ELISA (Fig. 3E-F) results showed that the expression of IL-18 and IL-1β was higher in the Model and Model + NC groups than in the Model group; the expression of IL-18 and IL-1β was lower in the HG + si-Impdh1 group than in the HG and HG + NC groups; and the differences were statistically significant ($P < 0.05$). These results suggested that silencing Impdh1 did play an

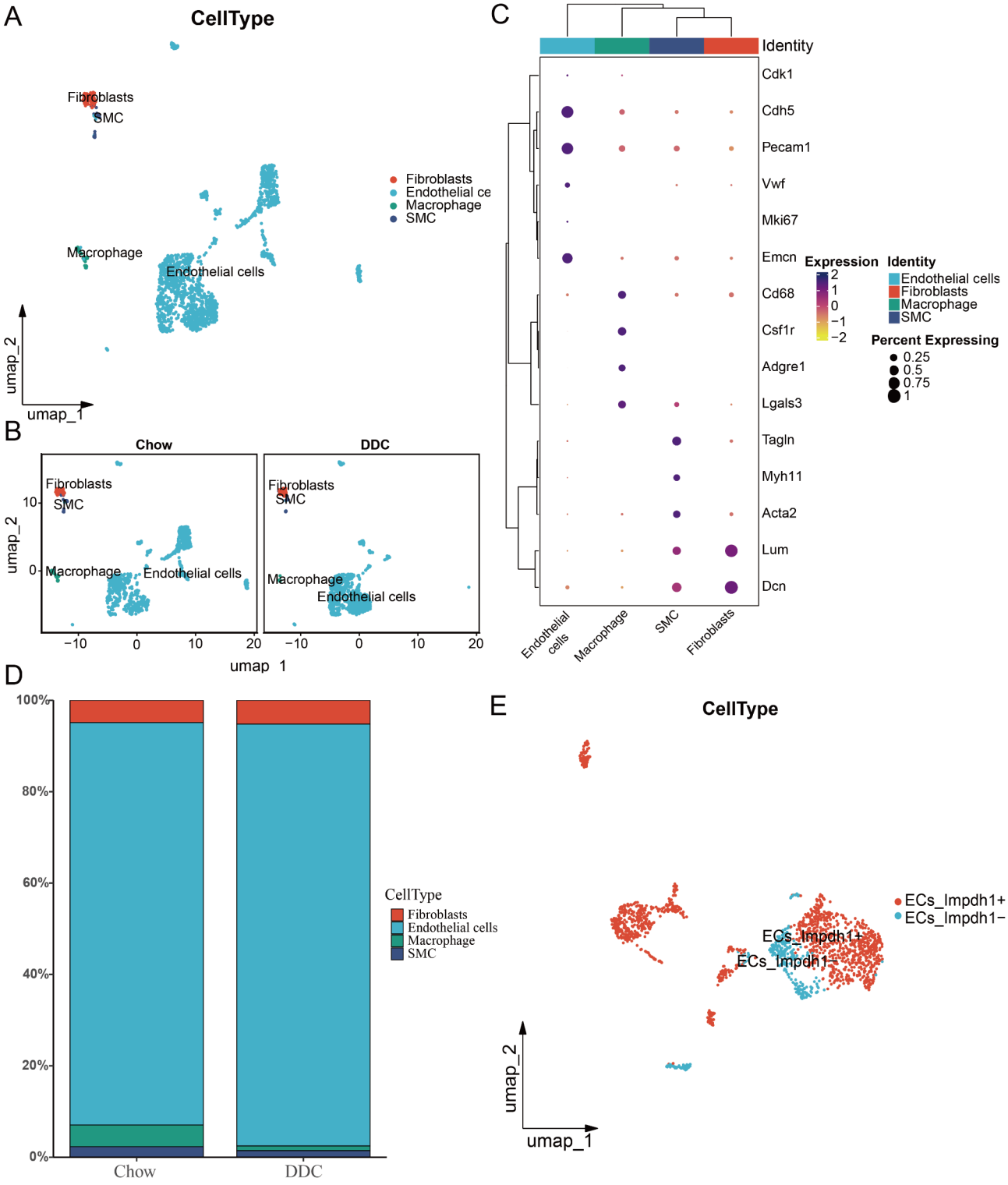

Fig. 1 Single-cell public dataset analysis. Note: **A**): UMAP plot of cell annotation results by cell type; **B**): UMAP plots of cell types for the DDC and Chow groups; **C**): Bubble plot of markers used to annotate cell types; **D**): Plot of the cell type proportion in the DDC and Chow groups; **E**): UMAP plot of EC subsets

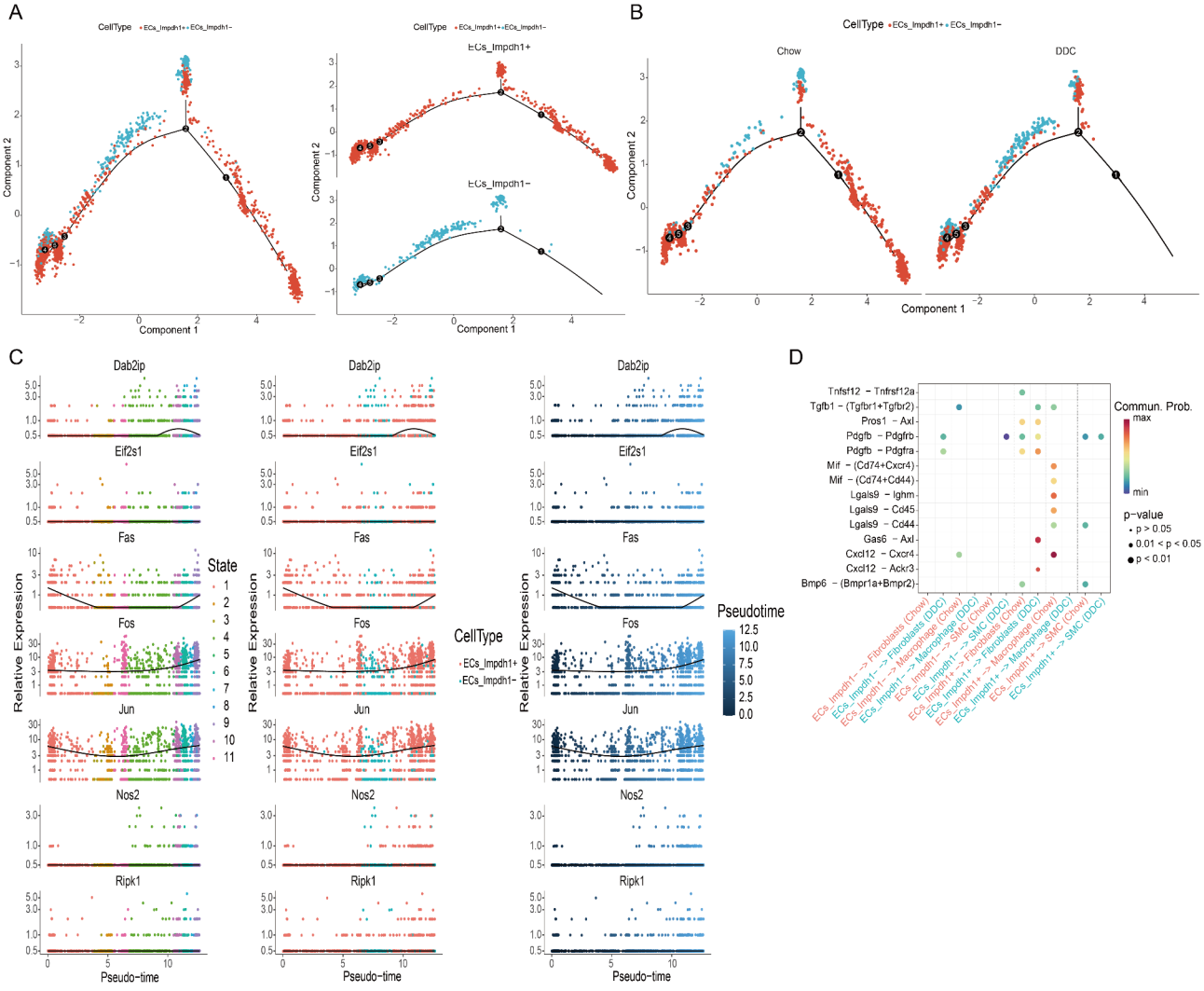

Fig. 2 Single-cell public dataset analysis. Note: **A)**: Distribution of different subsets of cells in the cell trajectory map. ECs_Impdh1^{+} (red dots) was mainly distributed at the end branches, while ECs_Impdh1^{-} (blue dots) was mainly at the start branches; **B)**: Trajectory distribution map of cells between the Chow and DDC groups. Trajectory analysis of the Chow group revealed that ECs_Impdh1^{+} (red dots) appears to diverge from ECs_Impdh1^{-} (blue dots); **C)**: Trajectory distribution map of cells between the Chow and DDC groups, displaying the genetic changes in EC subsets during differentiation; **D)**: Receptor^{-} ligand interaction between cells, displaying the signals sent by ECs_Impdh1^{-} and ECs_Impdh1^{+} to other cells, where the color and the circle size both represent their different correlations.

inhibitory role in the mechanism of pyroptosis in mouse aortic tissues.

Silencing Impdh1 can ameliorate HG-induced EC injury and pyroptosis

To elucidate the effect of Impdh1 on ECs, ECs were cultured with HG medium. qRT-PCR showed that Impdh1 expression was increased in HG-treated cells but decreased after transfection with si-Impdh1 (Fig. 4A), and the differences were all statistically significant ($P < 0.05$). CCK-8 assay results (Fig. 4B) revealed that cell viability was significantly reduced in the HG and HG + NC groups compared to the NG group. Furthermore, silencing Impdh1 can improve the down-regulation of cell viability in the presence of HG. IF staining results (Fig. 4C) showed that the OD values of NLRP3, pro-Caspase1, and GSDMD were significantly increased in the HG and HG + NC groups compared with those in the NG group, and that the OD values in the HG + si-Impdh1 group were significantly decreased compared with those in the Model and Model + NC groups. Cell scratch assay showed that HG can promote EC migration, whereas knocking down Impdh1 did just the opposite (Fig. 4D). Tube formation assay results (Fig. 4E) showed that compared with the NG group, the tube formation ability of the HG and HG + NC groups was significantly decreased. Whereas, silencing Impdh1 can improve the tube formation ability of ECs in the HG state. The ELISA results

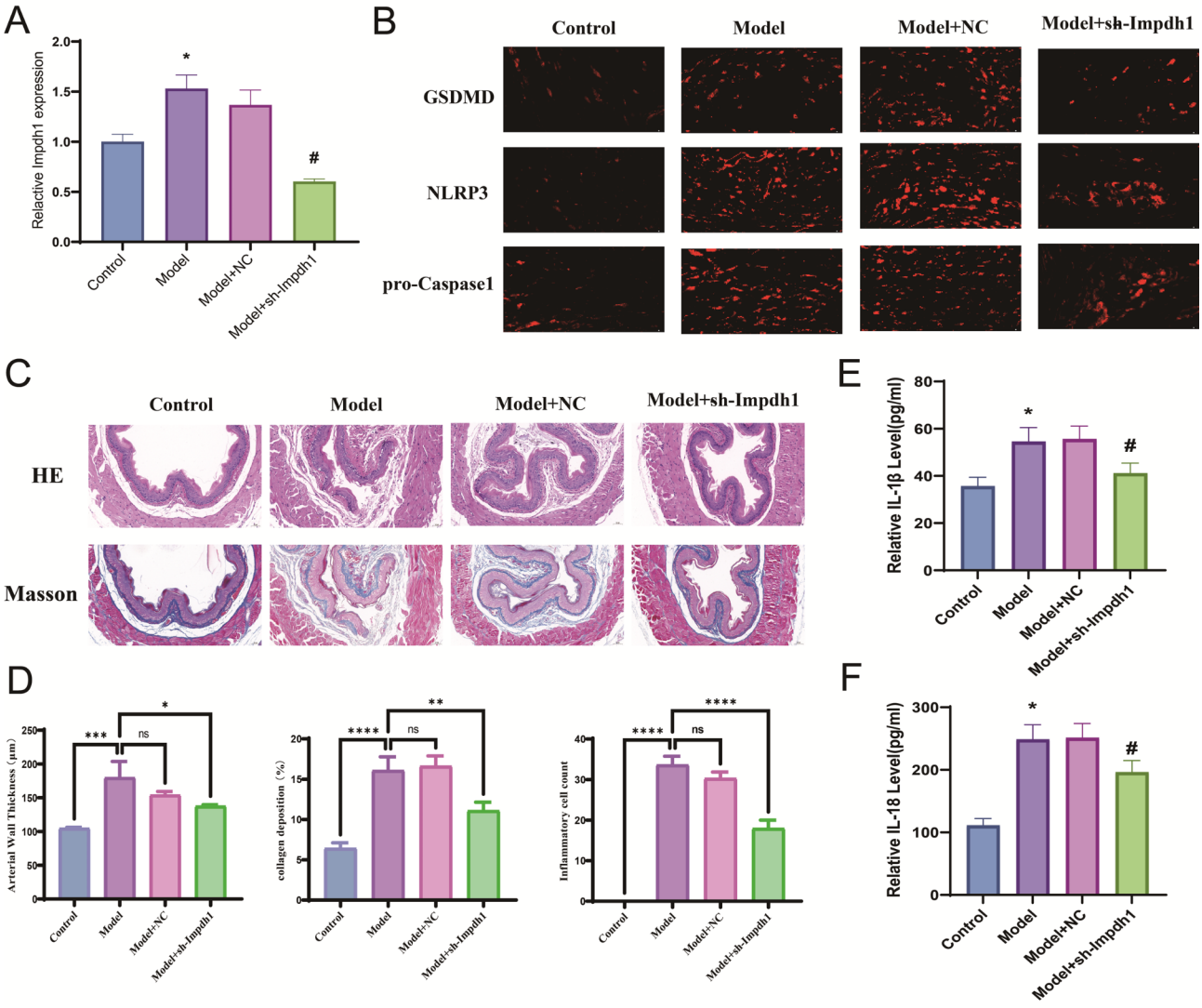

Fig. 3 Silencing Impdh1 can inhibit aortic tissue damage and pyroptosis in mice. Note: * indicated $P < 0.05$ compared with the Model group, # indicated $P < 0.05$ compared with the Model + NC group. **A**): qRT-PCR assay to determine Impdh1 expression in mice; **B**): IF staining plot to indicate GSDMD, pro-Caspase1, and NLRP3 expression; **C-D**): H&E and Masson staining after silencing of Impdh1 to demonstrate the pathological features of aorta in mice and relevant statistical results; **E-F**): ELISA to detect IL-18 and IL-1β levels

(Fig. 4F-G) showed that the expression of IL-18 and IL-1β in the HG and HG + NC groups was higher than that in the NG group; the expression of IL-18 and IL-1β in the HG + si-Impdh1 group was lower than that in the HG and HG + NC groups; and the differences were all statistically significant ($P < 0.05$). In summary, silencing Impdh1 can ameliorate HG-induced EC injury and pyroptosis.

Identification of DEGs by bulk RNA-seq and functional enrichment analyses of the DEGs

A total of 250 DEGs were obtained by bulk RNA-seq analysis, including 141 up-regulated and 109 down-regulated genes, and Impdh1 was significantly up-regulated in diabetic mice (Fig. 5A-B). GO analysis showed that the DEGs were mainly enriched in Immune response, Immune system process, BMP-binding protein, and Extracellular region (Fig. 5C). KEGG enrichment showed that the DEGs were enriched to pathways such as Drug metabolism-cytochrome P450, Motor proteins, Fluid shear stress, and Atherosclerosis (Fig. 5D). Impdh1 was highly correlated with pyroptosis-associated genes, such as Casp3, Casp8ap2, Nfkb1, and Tlr4, indirectly verifying the close association between Impdh1 and pyroptosis (Fig. 5E).

Discussion

DA is one of the most serious complications of DM. Angiopathy can lead to medial artery calcification of larger arteries, but its main effect is on the microcirculation [16]. Endothelial dysfunction is the initial and

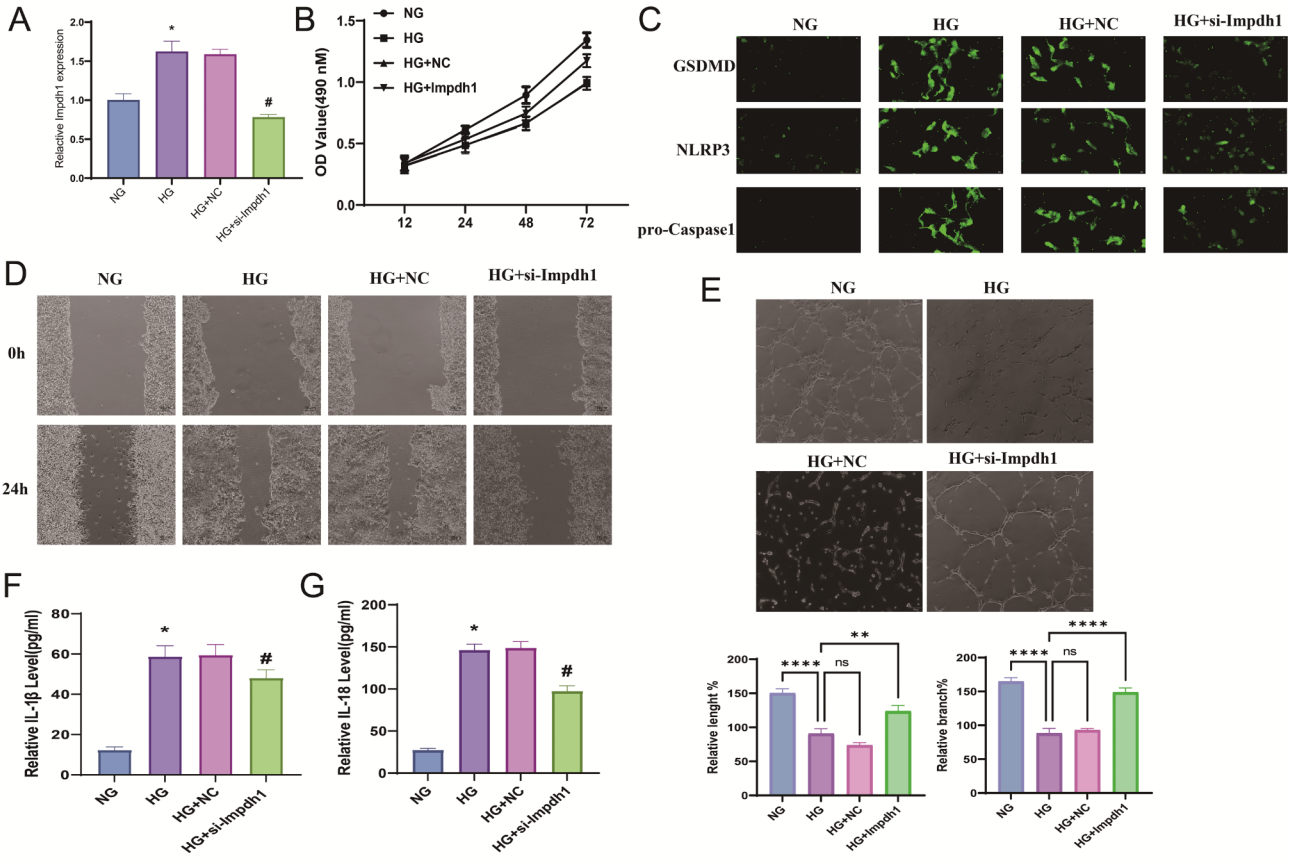

Fig. 4 Silencing Impdh1 can ameliorate HG-induced EC injury. Note: * indicated $P < 0.05$ compared with the NG group, # indicated $P < 0.05$ compared with the HG + NC group. **A**): qRT-PCR assay to determine Impdh1 expression in ECs; **B**): CCK-8 assay to detect the cell viability of ECs; **C**): IF staining plots to indicate the expression of GSDMD, pro-Caspase1, and NLRP3; **D**) Cell scratch assay to assess the migration ability; **E**) Tube formation assay; **F-G**): ELISA to detect IL-18 and IL-1β levels

operative step in the pathogenesis of diabetic vascular complications, where hyperglycemia and lipid metabolism disorders lead to endothelial dysfunction through direct metabolite damage, crosstalk between immunity and inflammation, and related interaction networks [17].

In the present study, scRNA-seq analysis revealed that Impdh1 was associated with DA and might participate in lesion development as a hub gene involved in pyroptosis. IMPDH is a rate-limiting enzyme in guanosine triphosphate (GTP) synthesis and assembles into filaments in cells to desensitize the enzyme to feedback inhibition and promote nucleotide production [18]. Impdh1, a key enzyme in the retina, is essential for the normal function of photoreceptor cells [19]. Diabetic retinopathy, on the other hand, is an important complication of DA [20], which might be caused by pigmentary degeneration of the retina through IMPDH1.

In the present study, cell-cell communication results demonstrated that Gas6-Axl was specifically expressed in the Impdh1^{+} subsets. Growth arrest-specific gene 6 (Gas6) and Anexelekto (AXL) receptor tyrosine kinase are involved in inflammatory diseases and participate in the development and progression of a range of malignancies and autoimmune diseases [21, 22]. There are few reports on the relationship between Impdh1 and DM. Therefore, the present study investigated the effect of Impdh1 on DA mice using in vivo and in vitro basic experiments and verified the finding by the obtained bulk RNA-seq data on the basis of scRNA-seq data. The basic experiments demonstrated that silencing Impdh1 can decrease the inflammatory cell infiltration in mouse aorta and the expression of NLRP3, GSDM, and caspase-1 in HG-treated ECs. In addition, it can also suppress inflammatory factors such as IL-1β and IL-18 and reduce pyroptotic cell death. Furthermore, bulk RNA-seq data revealed that Impdh1 was associated with the development of atherosclerosis and was closely related to the pyroptosis genes Casp3, Casp8ap2, Nfkb1, and Tlr4. This finding indirectly validated our previous findings. However, unfortunately, the bulk RNA-seq analysis revealed that the pyroptosis gene is Casp3, instead of Casp1 in the previous experimental validation. Pyroptosis is divided into CASP1-mediated classical pathway and CASP3/4/5/11-mediated non-classical pathway [23].

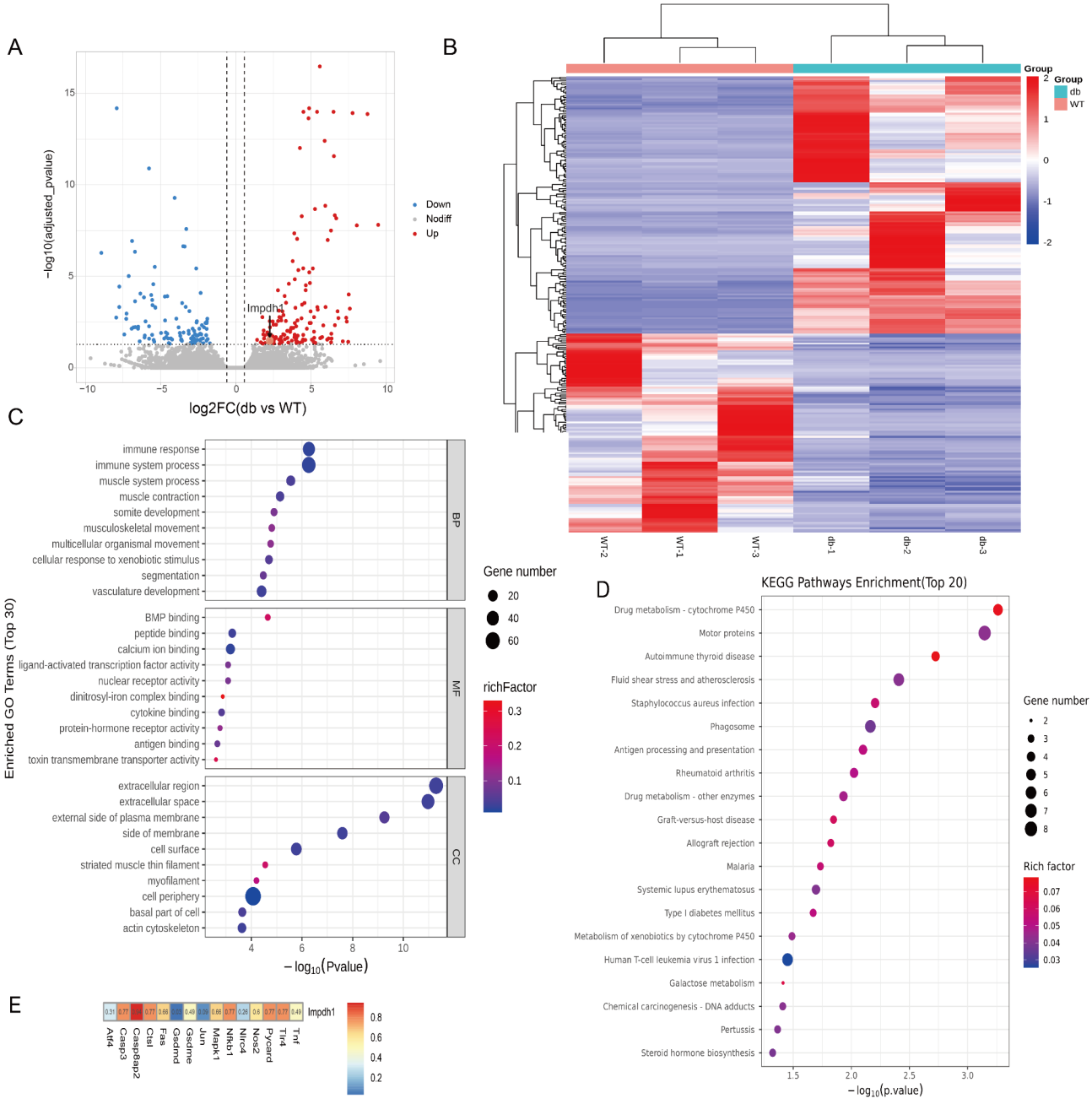

Fig. 5 Identification and functional enrichment analysis of DEGs in db/db and db/m mice. Note: **A**): Volcano plot of DEGs between the BLCA and Control in TCGA. Red dots represented up-regulated genes, and blue dots represented down-regulated genes; **B**): Heat map of the expression of DEGs; **C-D**): Enrichment bubble plots of GO and KEGG pathway of DEGs; **E**): Correlation map of Impdh1 with pyroptosis-related genes

Therefore, this finding only proved that Impdh1 is associated with EC pyroptosis and can not determine the specific pyroptosis pathway. It requires more experimental data to follow whether Impdh1 is a classical pathway, a non-classical pathway, or both pathways with unknown ratios of their occurrence.

In summary, Impdh1 is identified as a potential pyroptosis-related gene associated with DA by scRNA-seq and bulk RNA-seq and can protect aortic ECs by inhibiting pyroptosis and inflammation. There are some limitations in this study. Firstly, the limited scRNA-seq data in this study will affect the comprehensiveness and accuracy of the results, because they cannot represent the diversity of all cell types in the whole tissues or organs. Thus, we will try to collect as many samples as possible in the subsequent experiments to expand the scale and diversity of the dataset. Meanwhile, we will combine more experimental techniques to validate and analyze the results

from multiple perspectives in more animal models. In addition, this study found that Gas6-Axl signaling was specifically expressed in the Impdh1$^+$ EC subset. Gas6 belongs to the family of vitamin K-dependent coagulation proteins and can interact with the receptor tyrosine kinases of the Tyro-3, Axl, Mer (TAM) family. Gas6 has been reported to play a key role in neointimal formation, vasculitis, and atherosclerosis, highlighting its importance in vascular biology and disease [24, 25]. This finding indirectly confirms the importance of Impdh1$^+$ in diabetic vasculopathy. However, the experimental part of this study mainly focused on how Impdh1$^+$ advances diabetic vasculopathy by interfering with EC pyroptosis and didn't delve into its molecular mechanism. Thus, Gas6-Axl signaling can serve as a breakthrough point to carry out the subsequent research on the specific pathogenesis of diabetic vasculopathy. By exploring the role of Gas6-Axl signaling in the involvement of Impdh1$^+$ in the pathogenesis of diabetic vasculopathy, we are expected to provide stronger and better evidence in this field, thus promoting the in-depth development of related research.

Acknowledgements
The authors would like to thank OBiO Technology for their assistance in animal experiments.

Author contributions
RX, HG, TL wrote the main manuscript text and HX, CX prepared figures. All authors reviewed the manuscript.

Funding
This study was funded by the Natural Science Foundation of Sichuan (grant number: 2024NSFSC1855), the Scientific Research Project of Sichuan Administration of Traditional Chinese Medicine (grant number: 2023zd012) and the Xinglin Scholars Postdoctoral Special Program of Chengdu University of Traditional Chinese Medicine (grant number: BSH2021033).

Data availability
The datasets generated during the current study are available from the corresponding author on reasonable request.

Declarations

Ethics approval
All experiments involving animals were approved by the Animals Ethics Committee of OBiO Technology (Shanghai) Corp., Ltd. (Ethics approval number: IACAC-141).

Consent to participate
Not applicable.

Consent for publication
Not applicable.

Competing interests
The authors declare no competing interests.

Author details
[1]Hospital of Chengdu University of Traditional Chinese Medicine, Chengdu, Sichuan, China
[2]TCM Regulating Metabolic Diseases Key Laboratory of Sichuan Province, Chengdu, Sichuan, China

Received: 25 September 2024 / Accepted: 24 February 2025
Published online: 13 March 2025

References

1. Flyvbjerg A. Diabetic angiopathy, the complement system and the tumor necrosis factor superfamily. Nat Rev Endocrinol. 2010;6(2):94–101.
2. Stehouwer CD, Lambert J, Donker AJ, van Hinsbergh VW. Endothelial dysfunction and pathogenesis of diabetic angiopathy. Cardiovasc Res. 1997;34(1):55–68.
3. Jenkins AJ, Best JD, Klein RL, Lyons TJ. Lipoproteins, glycoxidation and diabetic angiopathy. Diabetes Metab Res Rev. 2004;20(5):349–68.
4. Xiang H, Song R, Ouyang J, Zhu R, Shu Z, Liu Y, Wang X, Zhang D, Zhao J, Lu H. Organelle dynamics of endothelial mitochondria in diabetic angiopathy. Eur J Pharmacol. 2021;895:173865.
5. Wang W, Lo ACY. Diabetic retinopathy: pathophysiology and treatments. Int J Mol Sci 2018, 19(6).
6. Wada J, Makino H. Inflammation and the pathogenesis of diabetic nephropathy. Clin Sci (Lond). 2013;124(3):139–52.
7. Mamun AA, Wu Y, Nasrin F, Akter A, Taniya MA, Munir F, Jia C, Xiao J. Role of pyroptosis in diabetes and its therapeutic implications. J Inflamm Res. 2021;14:2187–206.
8. Rao Z, Zhu Y, Yang P, Chen Z, Xia Y, Qiao C, Liu W, Deng H, Li J, Ning P, et al. Pyroptosis in inflammatory diseases and cancer. Theranostics. 2022;12(9):4310–29.
9. Yang F, Bettadapura SN, Smeltzer MS, Zhu H, Wang S. Pyroptosis and pyroptosis-inducing cancer drugs. Acta Pharmacol Sin. 2022;43(10):2462–73.
10. Wei Y, Yang L, Pandeya A, Cui J, Zhang Y, Li Z. Pyroptosis-Induced inflammation and tissue damage. J Mol Biol. 2022;434(4):167301.
11. Kaur R, Kaur M, Singh J. Endothelial dysfunction and platelet hyperactivity in type 2 diabetes mellitus: molecular insights and therapeutic strategies. Cardiovasc Diabetol. 2018;17(1):121.
12. Wang X, Wang W, Zhang R, Ma B, Ni L, Feng H, Liu C. Melatonin attenuates high glucose–induced endothelial cell pyroptosis by activating the Nrf2 pathway to inhibit NLRP3 inflammasome activation. Mol Med Rep 2023, 27(3).
13. Gimbrone MA Jr., García-Cardeña G. Endothelial cell dysfunction and the pathobiology of atherosclerosis. Circ Res. 2016;118(4):620–36.
14. Bremer S, Rootwelt H, Bergan S. Real-time PCR determination of IMPDH1 and IMPDH2 expression in blood cells. Clin Chem. 2007;53(6):1023–9.
15. Liu C, Zhang W, Zhou X, Liu L. IMPDH1, a prognostic biomarker and immunotherapy target that correlates with tumor immune microenvironment in pan-cancer and hepatocellular carcinoma. Front Immunol. 2022;13:983490.
16. McMillan DE. Diabetic angiopathy–its lessons in vascular physiology. Am Heart J. 1978;96(3):401–6.
17. Xue C, Chen K, Gao Z, Bao T, Dong L, Zhao L, Tong X, Li X. Common mechanisms underlying diabetic vascular complications: focus on the interaction of metabolic disorders, immuno-inflammation, and endothelial dysfunction. Cell Commun Signal. 2023;21(1):298.
18. Calise SJ, O'Neill AG, Burrell AL, Dickinson MS, Molfino J, Clarke C, Quispe J, Sokolov D, Buey RM, Kollman JM. Light-sensitive phosphorylation regulates retinal IMPDH1 activity and filament assembly. J Cell Biol 2024, 223(4).
19. Keppeke GD, Chang CC, Zhang Z, Liu JL. Effect on cell survival and Cytoophidium assembly of the adRP-10-related IMPDH1 missense mutation Asp226Asn. Front Cell Dev Biol. 2023;11:1234592.
20. Zhang H, Mo Y. The gut-retina axis: a new perspective in the prevention and treatment of diabetic retinopathy. Front Endocrinol (Lausanne). 2023;14:1205846.
21. Zhang S, Liu Y, Wang X, An N, Ouyang X. STAT1/SOCS1/3 Are Involved in the Inflammation-Regulating Effect of GAS6/AXL in Periodontal Ligament Cells Induced by Porphyromonas gingivalis Lipopolysaccharide In Vitro. J Immunol Res 2021, 2021:9577695.
22. Di Stasi R, De Rosa L, D'Andrea LD. Therapeutic aspects of the Axl/Gas6 molecular system. Drug Discov Today. 2020;25(12):2130–48.
23. Ling Y, Ren N, Yang Y, Xu H, Xiong H, Wang Q, Lu D, Yao X, Ma W. Kaempferol alleviates rheumatoid arthritis through pyroptosis based on bioinformatics analysis and experimental validation. Sci Rep. 2024;14(1):29769.
24. Lee CH, Shieh YS, Hsiao FC, Kuo FC, Lin CY, Hsieh CH, Hung YJ. High glucose induces human endothelial dysfunction through an Axl-dependent mechanism. Cardiovasc Diabetol. 2014;13:53.

25. Robins RS, Lemarié CA, Laurance S, Aghourian MN, Wu J, Blostein MD. Vascular Gas6 contributes to thrombogenesis and promotes tissue factor up-regulation after vessel injury in mice. Blood. 2013;121(4):692–9.

Publisher's note